Pressure-induced isostructural phase transformation in gamma-B(28)

Evgeniya Zarechnaya, Natalia Dubrovinskaia, Razvan Caracas, Marco Merlini, Michael Hanfland, Yaroslav Filinchuk, Dmitry Chernyshov, Vladimir Dmitriev, Leonid Dubrovinsky

Pressure-induced isostructural phase transformation in γ-B_{28}

Evgeniya Zarechnaya,[1] Natalia Dubrovinskaia,[2,3,*] Razvan Caracas,[4] Marco Merlini,[5] Michael Hanfland,[6] Yaroslav Filinchuk,[6] Dmitry Chernyshov,[6] Vladimir Dmitriev,[6] and Leonid Dubrovinsky[1]

[1]*Bayerisches Geoinstitut, Universität Bayreuth, 95440 Bayreuth, Germany*

[2]*Mineralphysik, Institut für Geowissenschaften, Universität Heidelberg, 69120 Heidelberg, Germany*

[3]*Lehrstuhl für Kristallographie, Physikalisches Institut, Universität Bayreuth, 95440 Bayreuth, Germany*

[4]*Ecole Normale Supérieure de Lyon, Laboratoire de Sciences de la Terre, Centre National de la Recherche Scientifique, 46, allée d'Italie, 69364 Lyon Cedex 07, France*

[5]*Dipartimento di Scienze della Terra, Universita degli Studi di Milano, Via Botticelli 23, 20133 Milano, Italy*

[6]*ESRF, Boîte Postale 220, 38043 Grenoble, France*

(Received 15 October 2010; revised manuscript received 24 October 2010; published 18 November 2010)

Isostructural phase transformations (ISPhTs) so far were reported only for heavy elements and their compounds with complex electronic and/or magnetic structures. Studies of one of the lightest elemental material, high-pressure boron γ-B_{28}, by means of *in situ* single-crystal x-ray diffraction and Raman spectroscopy reveal abrupt changes in the compressional behavior and Raman spectra at 40 GPa. Combined experimental and *ab initio* theoretical analysis of the structural and vibrational properties of γ-B_{28} suggests that the ISPhT under compression is due to the changes in the polarity of the covalent bonds between the boron atoms in the complex quasimolecular structure of γ-B_{28}.

DOI: 10.1103/PhysRevB.82.184111 PACS number(s): 61.50.Ks

I. INTRODUCTION

Isostructural phase transformations are particular cases of isosymmetric transformations and include discontinuous isostructural transitions and crossovers. They are rare, intriguing phenomena in solids often associated with a significant volume collapse, giant magnetoelastic coupling, or negative thermal expansion.[1–5] Elemental boron and boron-rich compounds have been given a particular scientific and technological attention because of their specific physical properties: high melting temperatures, a wide energy band gap, high hardness, strong absorbance of neutrons, etc. The structures of these materials are based on icosahedral units as a common feature. Even high pressure does not destroy the rigid units so that the very recently described high-pressure boron phase[6–8] γ-B_{28} consists of B_{12} icosahedra typical for rhombohedral α- and β-boron. Consisting of only B_{12} units, α-boron does not show any phase transitions on compression to at least 80 GPa at ambient temperature. The arrangement of B_{12} icosahedra in β-boron is complex and its structure contains partially occupied sites.[9,10] The β-boron is more compressible (the bulk modulus $K_{300}=185-210$ GPa) in comparison with α-boron ($K_{300}=213-224$ GPa).[11,12] The resistivity measurements[13] indicate a transformation from β-boron into yet unknown superconducting phase at about 160 GPa. At pressures above 8.5 GPa and temperatures higher than 1500 °C pure boron crystallizes as a γ-B_{28} phase with a *Pnnm* space group.[6–8] It contains 28 atoms in the unit cell. The structure consists of B_{12} icosahedra and B_2 dumbbells linked covalently[6,7] (Fig. 1). The γ-B_{28} phase was demonstrated[7] to be stable at least to 30 GPa and 2000 K. However, experimental information about the high-pressure behavior of the γ-B_{28} phase is so far limited. Here we present the results of the high-pressure Raman spectroscopy study of γ-B_{28} up to 105 GPa and its single-crystal x-ray diffraction over 65 GPa.

II. METHODS

Single crystals and polycrystalline aggregates of γ-B_{28} were grown as described in our previous publications (see Refs. 6 and 7).

A. Diamond-anvil cell experiments

In different runs the sample was clamped between diamond anvils with culets of 300, 250, or 120 μm in diameter. Rhenium (in the Raman spectroscopy experiments) or steel (in single-crystal x-ray diffraction experiments) gaskets were indented to the thickness of about 50 μm and holes with a diameter of 100 or 80 μm were drilled in the center. Small isometric pieces of the high-pressure boron phase synthesized in a multianvil apparatus were loaded into the holes along with ruby balls served as pressure markers. As a pressure transmitting medium Ne or He were loaded at 1.4 kbar

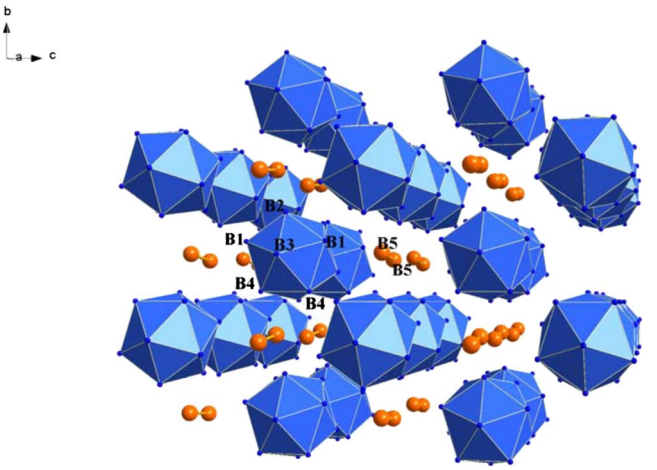

FIG. 1. (Color online) Structure of γ-B_{28} (atom labels are according to Ref. 6).

(all single-crystal x-ray diffraction experiments were performed in He pressure medium). One- and double-side laser annealing of samples compressed in Ne pressure medium at pressures above 20 GPa at temperatures up to 2000 K was conducted at BGI or at ESRF.

B. Raman spectroscopy

Raman spectroscopy studies were done on single crystals (with characteristic dimensions of $\sim 5\times 5\times 25$ μm^3) and polycrystalline aggregates of the B_{28} phase. Measurements were performed with LabRam and Dilor XY (DILOR GmbH) systems with a resolution better than 2 cm^{-1}. The 632.8 nm line of a He-Ne laser and 514 nm of an Ar laser were used for an excitation with a power at the sample position of 15–50 mW. The positions of Raman peaks were determined by processing experimental data using PEAKFIT© v4.12 software.

C. Single-crystal diffraction

Crystals with a size of about 7 $\mu m\times 7$ $\mu m\times 30$ μm were selected and measured at ID09a at the European Synchrotron Radiation Facility (ESRF). Diffraction data were collected at 293 K using the MAR555 image plate detector, radiation with a wavelength of 0.4143 Å and the crystal-to-detector distance of 399 mm. 120 frames in the omega scanning range of −30° to +30° were collected (0.5° scanning step size) with exposure time of 1 s. The data were processed using the CRYSALIS software [Oxford Diffraction (2006) CRYSALIS RED, version 1.171.31.8. Oxford Diffraction Ltd., Abingdon, Oxfordshire]. Crystal-structure refinements on integrated intensities were carried out with JANA2006 software.

D. *Ab initio* calculation

We performed first-principles calculations using the density-functional theory and density-functional perturbation theory formalisms as implemented in the ABINIT code.[14] We employed a $6\times 6\times 6$ regular grid of high special k points[15] and a kinetic-energy cutoff of 30 Ha (1 Ha=27.2116 eV). These ensured a precision on the order of 1 mHa in energy and better than 1 GPa in pressure. The calculations were performed on the JADE machine of CINES.

III. RESULTS

A. Raman spectroscopy at high pressure.

The γ-B_{28} gives very distinct and strong Raman spectra at ambient conditions[6,7,16] so that the Raman spectroscopy could be the most convenient and useful technique for investigation of the high-pressure behavior of this phase. Polarized Raman spectroscopy studies[16] allowed assigning vibration modes of γ-B_{28} thus creating a basis for the present study. Some examples of Raman spectra of polycrystalline γ-B_{28} collected at high pressure are presented in Fig. 2(a). The pressure dependence of Raman modes [Fig. 2(b)] can be shown in terms of the mode-Grüneisen parameter, defined as $\gamma_{\omega i}=-\partial \ln \omega_i/\partial \ln V=-(B_0/\omega_i)\partial\omega_i/\partial P$, where ω_i is the phonon frequency, B_0 is the bulk modulus (227 GPa at ambient conditions[7]), V is the molar volume, and P is the pressure. According to the values of the mode-Grüneisen parameters, all observed Raman peaks could be divided into three groups (Table I). To the first group belongs the mode B_{2g} at 319(3) cm^{-1} for which the Grüneisen parameter (2.8) is distinctly high. According to theoretical analysis (Table II) this mode is associated with tilts (rotations) around the a axis of the B_{12} icosahedra. The second group of mode consists of weakly varying (γ=0.03–0.2) narrow bands in the frequency

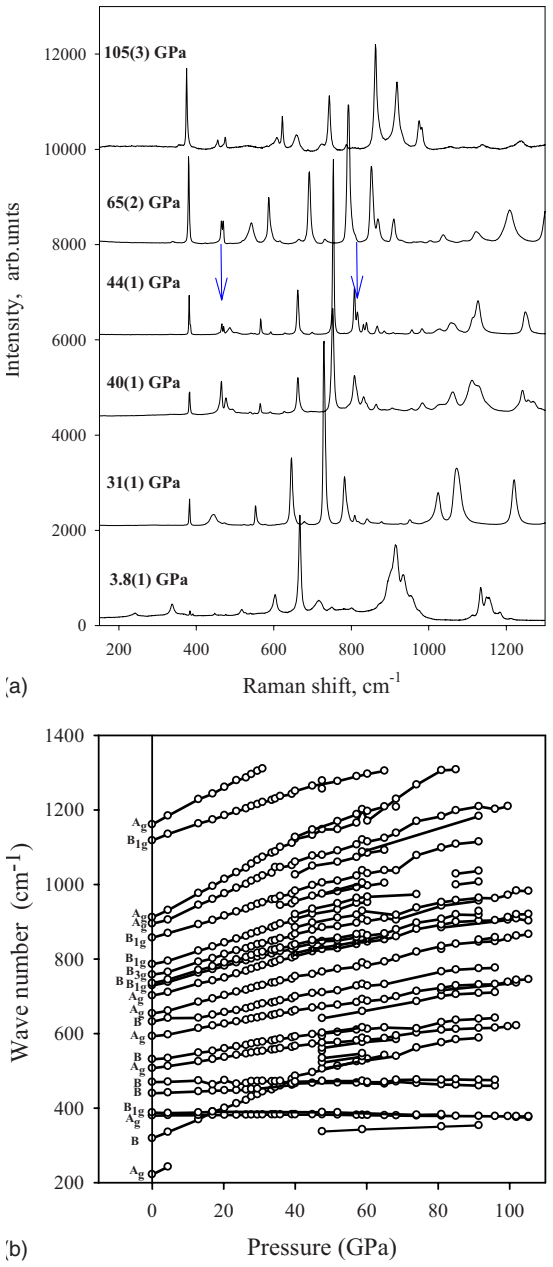

FIG. 2. (Color online) (a) Examples of Raman spectra of γ-B_{28} compressed in a neon pressure transmitting medium in a diamond-anvil cell. Arrows highlight some parts of the spectra which undergo rapid changes at pressure above 40 GPa. (b) Variation in the positions of Raman lines of γ-B_{28} as a function of pressure. Mode assignment at ambient conditions is given according to Ref. 16 [for some modes we could not assign their type (B_{2g} or B_{3g}) so that they were labeled with the symbol "B" (Ref. 16)].

TABLE I. Assignment of experimental (Ref. 16) and theoretical phonon frequencies at ambient conditions with experimentally determined mode-Grüneisen parameters (γ_{exp}).

Experiment				Theory	
ω_{exp} (cm^{-1})	Assignment	γ_{exp} below 39 GPa	γ_{exp} above 39 GPa	ω_{th} (cm^{-1})	Assignment
217(2)	B_{2g}, B_{3g}				
222(2)	A_g				
319(3)	B_{2g}, B_{3g} [a]	2.76	1.04	303	B_{2g}
380(1)	A_g	0.07	−0.03	387	A_g
388(2)	B_{1g}	0.17		389	B_{3g}
440(2)	B_{2g}, B_{3g}	0.20	−0.02	454	B_{3g}
460(2)	B_{1g} [a]			464/475	B_{3g}/B_{1g}
470(2)	B_{2g}, B_{3g}	0.03	−0.03	464/475	B_{3g}/B_{1g}
507(2)	A_g	0.65	0.34	536	A_g
531(2)	B_{2g}, B_{3g}	0.68		537	B_{2g}
593(3)	A_g	0.67	0.41	611	A_g
632(2)	B_{2g}, B_{3g}	0.53	0.42	585/575	B_{2g}/B_{3g}
654(2)	A_g	0.84	0.47	687	A_g
686(3)	B_{1g}, B_{2g}, B_{3g} [a]			658	B_{1g}
702(3)	A_g [a]	0.85	0.50	732	A_g
712(3)	B_{2g}, B_{3g}			714/719	B_{3g}/B_{2g}
729(2)	B_{1g}	0.78	0.40	726	B_{1g}
735(2)	B_{1g}, B_{2g}, B_{3g} [a]	0.79	0.42	735	B_{2g}
758(2)	B_{3g}	0.82	0.45	765	B_{3g}
786(2)	B_{1g}	0.87	0.54	781, 784	B_{1g}, B_{1g}
857(3)	B_{1g}	0.81	0.52	862	B_{1g}
878(2)	B_{1g}, B_{3g} [a]			884	B_{3g}
895(2)	A_g	1.05	0.55	887	A_g
912(2)	A_g	1.26	0.66	920	A_g
929(2)	A_g			970?[b]	A_g
952(2)	B_{2g}, B_{3g} [a]			959	B_{2g}
1095(2)	B_{1g}, B_{2g}, B_{3g} [a]				
1118(2)	B_{1g}	0.98	0.40	1118	B_{1g}
1138(2)	B_{1g}			1138	B_{1g}
1161(2)	A_g	0.42		1189	A_g
1189(2)	A_g			1194	A_g
1218(2)	A_g				

[a]Peaks which are visible also in forbidden scattering geometries (Ref. 16).
[b]The "?" marks the line whose assignment is ambiguous.

range 380–470 cm^{-1}. All these modes are assigned to vibrations of B_{12} icosahedra (380, 388, and 460 cm^{-1}) or both B_{12} icosahedra and B_2 dumbbells (444 and 470 cm^{-1}) along the unit-cell axes (Table II). Note that similar behavior of icosahedron and icosahedron-dumbbell vibrations were observed in α-boron,[17] in highly ordered pnictides ($B_{12}As_2$ and $B_{12}P_2$),[18] and boron carbide (B_4C).[19] The Grüneisen parameters of modes observed between 507 and 1200 cm^{-1} (the third group) are in the range of 0.42–1.05. These bands arise mainly from intraicosahedral vibrations, such as breathing or rocking-stretching modes. Note that apparent changes in the shape of spectra in the 800–1000 cm^{-1} region on compression to about 39 GPa (Fig. 2) are entirely due to differences in mode-Grüneisen parameters of the bands.

The observed high-pressure behavior of Raman modes can be qualitatively related to the response of the γ-B_{28} structure on compression. Indeed, rotations of B_{12} icosahedra, or of the B_{12} icosahedra and B_2 dumbbells around *b* and *c* axes (Fig. 1, Table II) require changes in the length of the shortest (i.e., strongest) B-B contacts between icosahedra and/or between an icosahedron and a dumbbell[7]; they correspond to the modes with the smallest mode-Grüneisen parameters. The mode which is most sensitive to the volume changes is associated with the rotation of B_{12} icosahedra

TABLE II. Calculated Raman-active modes of γ-B_{28} at 0 GPa.

Assignment	ω_{calc}(cm^{-1})	Description
A_g	387	The B_6 half-caps move up and down and the whole B_{12} icosahedron tilts around the *c* axis 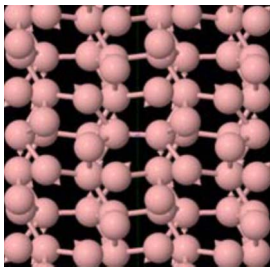
A_g	536	B_2 dumbells tilt around the *c* axis; slight participation of the B_{12} icosahedra that tilt much less
A_g	611	Breathing mode of the B_{12} icosahedra
A_g	687	Breathing mode of the B_{12} icosahedra
A_g	732	Tilt of B_2 associated with a movement of the B atoms from the sides of the B_{12} icosahedra, looking like a dangling bond; the B atoms from the B_{12} that move are the furthest apart from B_2
A_g	770	Breathing mode of the B_{12} icosahedra
A_g	811	Breathing mode of the B_{12} icosahedra; here the B atoms from the side, the ones that form a bond perpendicular to the B_2-B_{12} plane participate in the motion 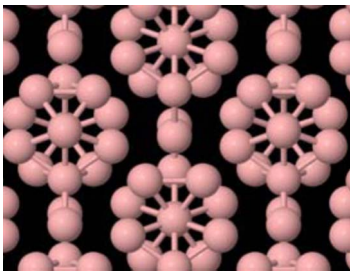
A_g	887	Breathing mode of the B_{12} icosahedra
A_g	920	Breathing mode of the B_{12} icosahedra 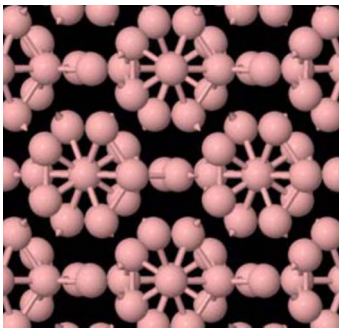
A_g	970	Breathing mode of the B_{12} icosahedra
A_g	1119	Tilt of the B_2 dumbell associated with a displacement of the two B atoms from the B_{12} icosahedra situated closest to the B_2 dumbells along the *b* axis
A_g	1194	Breathing-like mode of the B_{12} icosahedra dominated by the movement of

TABLE II. (*Continued.*)

		the apex atoms (these are the only ones that really move)
B_{1g}	**475**	Tilts of the B_{12} icosahedra around the *c* axis
B_{1g}	**554**	Tilts of the B_2 dumbells
B_{1g}	**658**	Vibration corresponding to half the B_{12} icosahedra vibrating against the other half along the *b* axis 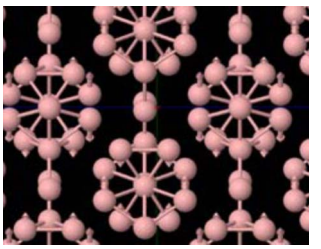
B_{1g}	**726**	Breathing mode of the B_{12} icosahedra
B_{1g}	**781**	Breathing mode of the B_{12} icosahedra; each half-cap breathes independently 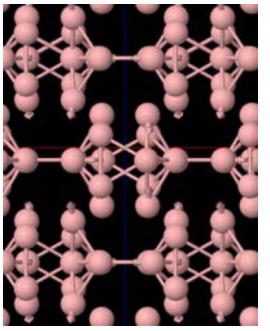
B_{1g}	**784**	Breathing mode of the B_{12} icosahedra; each half-cap breathes indepedently; the movement has an important *a* component, the sizes of the half-caps rotating around the z axis
B_{1g}	**793**	Breathing mode of the B_{12} icosahedra; dominated by a tilt of the B-B bond between the B_{12} icosahedra, in the (010) plane
B_{1g}	**862**	Breathing mode of the B_{12} icosahedra; B_2 do not participate
B_{1g}	**906**	Dominated by B_2 extension mode with some smaller participation from the breathing of B_{12} icosahedra from the B_2 side bonds parallel to the *c* axis
B_{1g}	**979**	Breathing mode of the B_{12} icosahedra, with lateral extension in the (100) planes 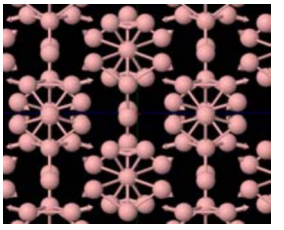
B_{1g}	**1118**	Tilt of the B_2 dumbell associated with a displacement of the two B atoms from the B_{12} icosahedra situated closest to the B_2 dumbbells along the *b* axis
B_{1g}	**1189**	Breathing-like mode of the B_{12} icosahedra dominated by the movement of the apex atoms (these are the only ones that really move)
B_{2g}	**303**	Tilts (=rotations) of the B_{12} icosahedra along the x axis
B_{2g}	**454**	Tilts (rotations) of the B_{12} icosahedra and of the B_2 dumbells. The B_{12} icosahedra around the *a* axis, while the B_2 dumbbells have a component along the *b* axis

TABLE II. (*Continued.*)

B_{2g}	**537**	Tilts of the B_{12} icosahedra around the *b* axis 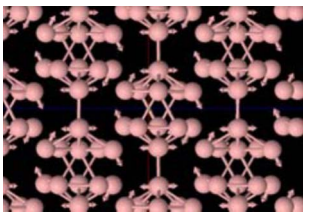
B_{2g}	**585**	Tilts of the B_{12} icosahedra around the *a* axis
B_{2g}	**719**	Shear-like mode of the B_{12} icosahedra; such that each half of the cage tilts around the *b* axis producing a sheared final B_{12} cage 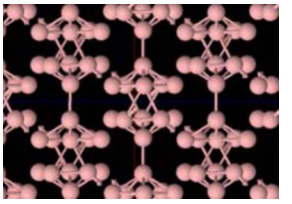
B_{2g}	**735**	Shear-like mode of the B_{12} icosahedra; the tilt system is slightly different than from the previous mode; there are two subunits within each half that tilt in anti-phase 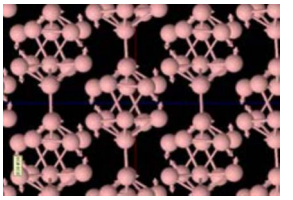
B_{2g}	**771**	The apex of the B_{12} atoms along the X axis and the B_2 dumbbells vibrate around the *b* axis
B_{2g}	**880**	Dominated by a tilt system of the B_{12} apex against the B_2 dumbbells
B_{2g}	**959**	Shear mode of the B_{12} icosahedra, associated with a tilt of the half-caps along the *b* axis
B_{3g}	**389**	Tilt mode of the B_{12} icosahedra around the *b* axis
B_{3g}	**403**	Tilt of the B_2 dumbbells with a sight participation from the B_{12} unit that tilt as well
B_{3g}	**464**	Another tilt of both B_{12} and B_2 around the *a* axis
B_{3g}	**575**	Shear mode of the B_{12} icosahedra; half-caps vibrate against the other half with a tilt around the *b* axis
B_{3g}	**714**	Double shear of the B_{12} icosahedra; the mode is dominated by the B_2 bond parallel to the *c* axis
B_{3g}	**765**	Breathing mode of the B_{12} icosahedra 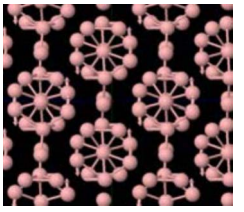
B_{3g}	**810**	Breathing mode of the B_{12} icosahedra, associated with a shear due to differential displacement in the (100) plane soft the different B of B_{12} icosahedra
B_{3g}	**884**	Breathing mode of the B_{12} icosahedra, associated with a shear due to differential displacement along the *a* axis of the different B of B_{12} icosahedra; dominated by lateral displacement of the apex atoms
B_{3g}	**929**	Complex breathing mode of the B_{12} icosahedra

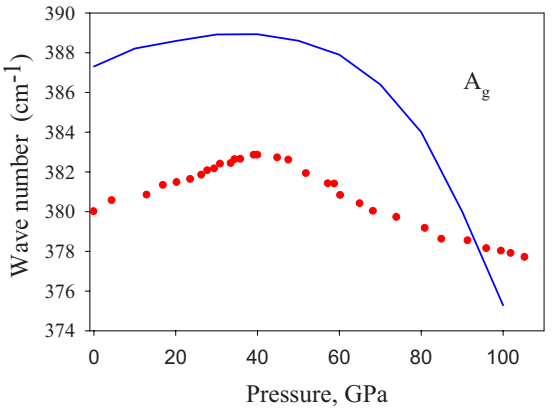

FIG. 3. (Color online) Example of the measured (dotted curve) and calculated (solid curve) Ag Raman mode as a function of pressure.

around the *a* axis and does not involve tension of the shortest interatomic contacts.

Most the Raman modes monotonically shift to higher wave numbers with increasing pressure up to about 35 GPa. At pressures higher than 40 GPa in all three independent experiments we observed an inflection in the modes behavior [Fig. 2(b), Table I]. Under further compression to pressures about 40–45 GPa several broaden peaks split (Fig. 2(a)). Although above ~40 GPa we detect up to 32 Raman modes in the spectra, the total number of modes was always less than 42 allowed in orthorhombic γ-B_{28}.[16] At the same pressure two modes (A_g at 380 cm^{-1} and B_{3g} at 470 cm^{-1}) drastically change their behavior and become soft with Grüneisen parameters of about −0.03 (Fig. 2; Table I, Fig. 3).

Phonon determination based on first-principles calculations show that the lowest six Raman modes (one A_g, one B_{1g}, two B_{2g}, and two B_{3g}) present pressure softening in perfect agreement with the experimental observations. They are lattice modes corresponding mainly to tilts of the B_{12} icosahedra. In particular, the behavior of the lowest B_{2g} mode is relevant as it hardens up to about 50 GPa and it softens beyond that pressure.

Laser annealing at 1500–1800 K at pressures above 40 GPa does not affect the Raman spectra and the changes are fully reversible on decompression suggesting that the orthorhombic γ-B_{28} may undergo a phase transition at high pressures. In order to test this hypothesis we have undertaken an intensive x-ray diffraction investigation of γ-B_{28} under compression.

B. Single-crystal x-ray diffraction at high pressure

Being the fifth element in the Periodic Table, boron is a very weak x-ray scatterer. X-ray powder-diffraction experiments on boron phases above 30 GPa are difficult[7,19] and could hardly provide even accurate lattice parameters. At the same time, single-crystal studies allowed investigating the behavior of lattice parameters of β-boron at pressure up to 100 GPa.[12] In three independent diamond-anvil cell (DAC) experiments we compressed single crystals of γ-B_{28} (grown in a multianvil apparatus in metallic fluxes[20]) to pressures over 65 GPa using He as a quasihydrostatic pressure transmitting medium. The collected x-ray diffraction data were sufficient in quality to refine both lattice parameters and atomic coordinates (Table III). Remarkably, the quality of the structural refinement based on the data collected in DACs was not worse than that based on the data obtained at ambient conditions (Table III), and it also proves that the crystals were in a good quasihydrostatic environment to highest pressures reached.

Up to the highest pressure reached in this study (65 GPa) all observed reflections perfectly match the γ-B_{28} (space group *Pnnm*) structure (Table III). However, the compressional behavior of the material at pressures below and above about 40 GPa is considerably different (Fig. 4). It manifests in an abrupt increase in the stiffness of the structure (more than 20% increase in the bulk modulus) and in the relative softening along the *a* axis in comparison with the *c* and especially the *b* axes. There is a clear change in the behavior of the *b*/*a* ratio (it decreases monotonously to about 35 GPa and increases above 40 GPa), and there is a discontinuity in "*F*-*f*" plot (normalized stress vs Eulerian strain, see insets in Fig. 4). An extrapolation of molar volumes of low-pressure and high-pressure materials to ambient conditions gives a difference of about 3% (Fig. 4).

On compression up to 40 GPa the shortest bond lengths as well as the average distances between any atom and its neighbors ("atom's sphere radius" as defined in IVTON software[22]) homogeneously decrease; their compressibilities are linear with values in the 0.019–0.024 GPa^{-1} range (Fig. 5). The volume of the B_{12} icosahedra also decreases smoothly to 40 GPa (Fig. 6). However the bulk modulus of this polyhedron (285 GPa) is significantly higher than the bulk modulus of the bulk material (227 GPa) confirming a molecular-solidlike behavior with intericosahedral bonding weaker than intraicosahedral ones. At pressures above 40 GPa the compressibility of the spheres around the B1 and B4 atoms (Fig. 1 for designation of atoms) does not change (these two atoms are not involved into the shortest intericosahedral contacts or into the contacts of the B_2 dumbbells and the B_{12} icosahedra). Contrary, the atoms involved in intraicosahedral bonding (labeled B3) or in bonding between the B_{12} icosahedra and the B_2 dumbbells (labeled B2 and B5) show pronounced changes in the compressional behavior. In parallel the B_{12} icosahedra become much more incompressible, exhibiting a 1/3 increase in the bulk modulus (Fig. 6).

IV. DISCUSSIONS

Both the Raman spectroscopy and the single-crystal x-ray diffraction studies reveal the existence of *two states* of γ-B_{28} with a pronounced difference in their vibrational and compressional properties. The abrupt change in the properties occurs at pressures ~40 GPa. However, neither the symmetry nor the structure change was detected in this pressure range. We conclude, therefore, that B_{28} undergoes an *isostructural* phase transformation.

Isostructural phase transformations are relatively exotic phenomena. They were reported for a few elements, in particular, in Ce (a well-known example of the isostructural

TABLE III. Structural parameters of the γ-B_{28} phase (*Pnnm*, $Z=28$) as revealed by single-crystal diffraction experiments in diamond-anvil cells at high pressures.

Run	Pressure (GPa)	Lattice parameters (Å)			Atomic coordinates					R_1(%) wR_2 (%)
		a	*b*	*c*	B1 8h	B2 4g	B3 4g	B4 8h	B5 4g	
B4_1	16.1(2)	4.9554(3)	5.5097(8)	6.8011(6)	0.1540(5) 0.5927(7) 0.7902(5)	0.6498(7) 0.7264(11) 0.5	0.3358(7) 0.5082(9) 0.0	0.8395(5) 0.7188(7) 0.8731(5)	0.6698(7) 0.9803(10) 0.0	7.57 8.07
B4_2	22.6(2)	4.9231(4)	5.4720(14)	6.7388(10)	0.1545(5) 0.5920(7) 0.7898(5)	0.6513(8) 0.7242(11) 0.5	0.3355(7) 0.5071(10) 0.0	0.8406(6) 0.7181(6) 0.8731(7)	0.6698(7) 0.9793(10) 0.0	6.39 7.12
B4_3	30.2(3)	4.8767(3)	5.4260(12)	6.6606(9)	0.1538(6) 0.5914(8) 0.7895(6)	0.6518(9) 0.7234(13) 0.5	0.3359(9) 0.5066(11) 0.0	0.8411(7) 0.7178(9) 0.8733(6)	0.6698(8) 0.9769(12) 0.0	6.92 8.18
B4_4	35.5(3)	4.8535(4)	5.4025(13)	6.6187(10)	0.1534(6) 0.5902(7) 0.7885(5)	0.6514(7) 0.7231(10) 0.5	0.3371(7) 0.5082(9) 0.0	0.8404(6) 0.7184(7) 0.8723(5)	0.6691(7) 0.9776(9) 0.0	4.68 5.21
B4_5	37.8(3)	4.8346(3)	5.3831(9)	6.5920(6)	0.1541(6) 0.5910(8) 0.7884(5)	0.6519(8) 0.7229(12) 0.5	0.3358(8) 0.5072(10) 0.0	0.8410(6) 0.7188(8) 0.8724(5)	0.6703(8) 0.9766(11) 0.0	6.02 6.92
B4_6	45.1(3)	4.8078(5)	5.3532(17)	6.5465(13)	0.1537(6) 0.5902(8) 0.7878(5)	0.6513(8) 0.7230(11) 0.5	0.3367(7) 0.5072(9) 0.0	0.8406(6) 0.7187(7) 0.8719(5)	0.6701(7) 0.9765(10) 0.0	5.46 5.62
B5_1	0.001	5.0508(2)	5.6181(4)	6.9793(5)	0.1543(4) 0.5928(5) 0.7930(4)	0.6481(6) 0.7279(7) 0.5	0.3357(5) 0.5072(6) 0.0	0.8386(4) 0.7195(5) 0.8737(4)	0.6695(5) 0.9834(7) 0.0	6.61 7.43
B5_2	5.8(1)	5.0115(5)	5.5731(10)	6.9041(12)	0.1542(4) 0.5921(5) 0.7917(3)	0.6485(6) 0.7267(7) 0.5	0.3355(5) 0.5059(6) 0.0	0.8390(4) 0.7195(4) 0.8733(4)	0.6701(5) 0.9820(7) 0.0	5.58 6.74
B5_3	9.6(2)	4.9810(2)	5.5392(3)	6.8535(4)	0.1542(5) 0.5924(6) 0.7914(4)	0.6483(6) 0.7277(8) 0.5	0.3364(6) 0.5079(7) 0.0	0.8392(4) 0.7198(5) 0.8731(4)	0.6699(6) 0.9813(7) 0.0	6.28 7.59
B5_4	14.7(2)	4.9636(2)	5.5192(4)	6.8160(5)	0.1542(6) 0.5921(7) 0.7907(5)	0.6487(8) 0.7264(9) 0.5	0.3357(7) 0.5082(8) 0.0	0.8392(5) 0.7193(6) 0.8728(5)	0.6710(7) 0.9798(8) 0.0	7.86 8.58
B5_5	15.1(2)	4.9267(2)	5.4751(4)	6.7439(6)	0.1538(6) 0.5907(6) 0.7893(4)	0.6499(9) 0.7253(8) 0.5	0.3353(8) 0.5064(7) 0.0	0.8403(6) 0.7184(5) 0.8722(5)	0.6718(8) 0.9779(7) 0.0	5.42 5.95
B5_6	21.5(2)	4.8986(4)	5.4462(9)	6.6990(11)	0.1544(4) 0.5910(4) 0.7887(3)	0.6494(7) 0.7244(7) 0.5	0.3357(6) 0.5076(6) 0.0	0.8401(4) 0.7188(4) 0.8717(4)	0.6712(6) 0.9779(6) 0.0	5.65 6.26
B5_7	26.5(2)	4.8715(3)	5.4189(6)	6.6651(7)	0.1550(11) 0.5930(13) 0.7891(8)	0.6481(18) 0.7187(16) 0.5	0.3352(14) 0.5092(13) 0.0	0.8389(10) 0.7146(10) 0.8732(9)	0.6707(16) 0.9818(16) 0.0	10.17 15.55
B5_8	31.7(3)	4.8492(5)	5.3910(10)	6.6116(13)	0.1542(5) 0.5912(7) 0.7873(5)	0.6494(7) 0.7239(9) 0.5	0.3356(7) 0.5098(9) 0.0	0.8402(5) 0.7194(7) 0.8714(5)	0.6712(7) 0.9756(9) 0.0	6.79 7.56
B5_9	36.2(3)	4.8246(6)	5.3679(12)	6.5713(11)	0.1539(4) 0.5906(5) 0.7871(3)	0.6495(6) 0.7240(7) 0.5	0.3358(6) 0.5093(7) 0.0	0.8409(4) 0.7189(5) 0.8713(4)	0.6710(6) 0.9758(7) 0.0	4.63 5.72
B5_10	41.2(3)	4.8100(2)	5.3531(5)	6.5486(5)	0.1542(5) 0.5905(6) 0.7867(3)	0.6494(7) 0.7235(8) 0.5	0.3357(7) 0.5089(7) 0.0	0.8408(5) 0.7182(6) 0.8711(4)	0.6716(7) 0.9754(7) 0.0	5.13 6.08
B5_11	45.0(3)	4.7857(3)	5.3291(7)	6.5091(7)	0.1544(6) 0.5909(6) 0.7862(4)	0.6498(8) 0.7227(8) 0.5	0.3366(7) 0.5086(7) 0.0	0.8407(5) 0.7180(6) 0.8709(5)	0.6710(7) 0.9749(7) 0.0	5.02 5.98

TABLE III. (*Continued.*)

Run	Pressure (GPa)	Lattice parameters (Å)			Atomic coordinates					R_1(%) wR_2 (%)
		a	*b*	*c*	B1 8h	B2 4g	B3 4g	B4 8h	B5 4g	
B5_12	51.2(4)	4.7208(5)	5.2508(12)	6.4015(14)	0.1543(11) 0.5912(12) 0.7858(9)	0.6529(17) 0.7214(14) 0.5	0.3340(13) 0.5076(13) 0.0	0.8401(10) 0.7168(11) 0.8703(8)	0.6731(14) 0.9729(12) 0.0	7.54 8.70
B5_p1	65.3(5)	4.731(3)	5.280(5)	6.4285(39)	0.1533(12) 0.5891(9) 0.7844(6)	0.6521(16) 0.7204(10) 0.5	0.3341(15) 0.5082(9) 0.0	0.8425(9) 0.7190(7) 0.8729(8)	0.6705(15) 0.9763(10) 0.0	6.94 6.91
B5_p2	55.6(5)	4.772(3)	5.318(5)	6.486(7)	0.1541(2) 0.5901(6) 0.7859(4)	0.6506(9) 0.7221(7) 0.5	0.3369(7) 0.5079(8) 0.0	0.8415(6) 0.7190(1) 0.8712(4)	0.6723(8) 0.9760(7) 0.0	5.55 5.60
B28[7]	0.001	5.0576(4)	5.6245(8)	6.9884(10)	0.1539(3) 0.5938(2) 0.7924(2)	0.6469(4) 0.7284(4) 0.5	0.3362(4) 0.5076(4) 0.0	0.8391(3) 0.7189(3) 0.8737(2)	0.6690(4), 0.9823(4) 0.0	3.73% 11.5%

transition,[1] see Ref. 23 for review) at high pressures, Zr and[24] Os.[25] However, established cases of the ISPhTs are related to the elements or compounds containing elements with the variable chemical valence due to fully or partially free *d*- or/and *f*-electronic shells (for example, SmS,[26] $EuCo_2P_2$,[27] rare-earth chalcogenides[28] and pnictides, see Ref. 29 for review), or/and materials which undergo magnetic or spin transitions, for example, MnO (Ref. 30) or YCo_5.[2] Boron is an element of the second row of the Periodic Table and the conventional mechanisms of the ISPhT in its crystal structure are highly unlikely (indeed, theoretical calculations[7,8] do not indicate any significant changes in band structure of γ-B_{28} at least to 100 GPa). At the same time γ-B_{28} is a quasimolecular material. The detailed single-crystal x-ray diffraction study conducted at ambient pressure[7] revealed the strong polar-covalent bonding with an electron density excess at B2 and B4 atoms (they belong to the B_{12} icosahedra) and an electron density deficit at B5 atoms (which form B_2 dumbbells). This suggests that the ISPhT in γ-B_{28} can be a result of changes in the electron density distribution between boron atoms and/or bonds or, in other words, changes in the character of chemical bonding. For compounds with the polar-covalent bonding, the splitting of the IR longitudinal- and transversal-optical (LO-TO) phonon modes can be used as a measure of the degree of the charge transfer,[8,9,31] which can be characterized by the generalized Lyddane-Sachs-Teller (LST) parameter $\xi=\Pi_i^n(\omega_i^{LO}/\omega_i^{TO})^2$. Using calculated values of frequencies for all IR-active modes at different pressures (Fig. 7) we found that above 50 GPa, in strict similarity with experimental data

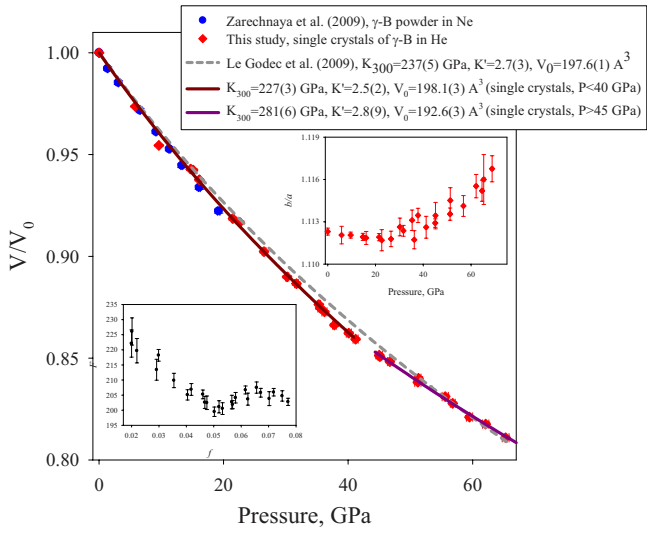

FIG. 4. (Color online) The relative unit-cell volume of γ-B_{28} as a function of pressure (red diamonds—single-crystal data from this study; blue circles—powder-diffraction data (Ref. 7); lines are fits with the third-order Birch-Murnaghan (BM3) equation of state: dark red for single-crystal data below 40 GPa, dark purple for single-crystal data above 45 GPa, and dashed line as reported by Le Godec *et al.* (Ref. 21) based on powder x-ray diffraction data to 70 GPa. Insets show the variation in the ratio of the lattice parameters b/a as a function of pressure and the *F*-*f* plot (normalized stress vs Eulerian strain).

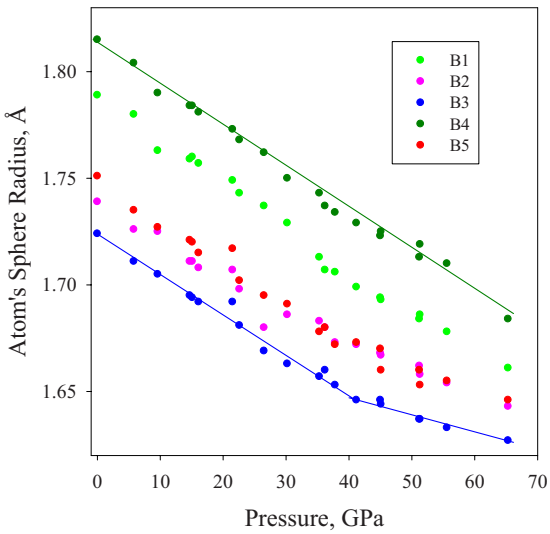

FIG. 5. (Color online) The average distance of the atom from its neighbors ["sphere radius," as defined in IVTON software (Ref. 22)] as a function of pressure. Continuous lines for B3 and B4 atoms are guide for eyes.

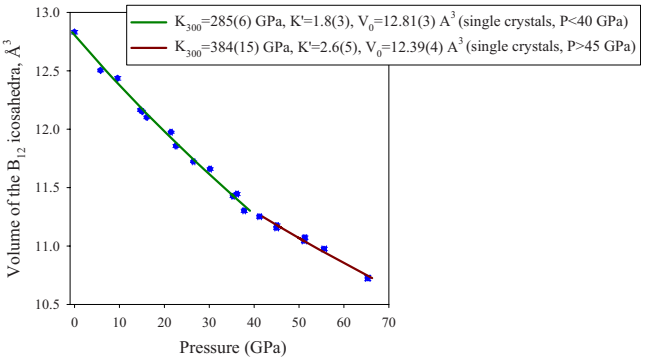

FIG. 6. (Color online) Volume of the B_{12} icosahedra as a function of pressure (blue dots). The polyhedron volumes were calculated in IVTON program (Ref. 22). Lines are fits with the BM3 equation of state: dark green for single-crystal data below 40 GPa, dark red for single-crystal data above 45 GPa.

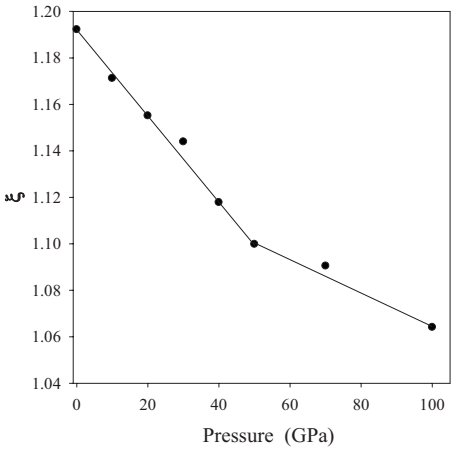

FIG. 7. The generalized Lyddane-Sachs-Teller parameter $\xi=\Pi_i^n(\omega_i^{LO}/\omega_i^{TO})^2$ of γ-B_{28} (ω_i^{LO} and ω_i^{TO} are calculated frequencies of longitudinal- and transversal-optical IR-active modes) as a function of pressure. The decrease in ξ with pressure indicates that the covalent bonding in γ-B_{28} becomes less polar under compression.

on changes in Raman spectra and compressional behavior, the LST parameter changes its pressure dependence. This result strengthens our assignment of the isostructural phase transformation in γ-B_{28} as due to alteration the polarity of the covalent bonding between the boron atoms in the complex quasimolecular structure.

Boron-rich carbides, nitrides, oxides, and borides of light elements with polar covalent and/or partially ionic bonding represent a large group of materials with prospective applications due to a number of unusual and potentially useful properties.[9,17] Our finding of the ISPhT in γ-B_{28} suggests that the same or similar mechanism, involving rapid pressure- or chemically induced changes in chemical bonding, could drive isostructural transformations in other boron-rich phases as well.

ACKNOWLEDGMENTS

We thank S. van Smaalen, S. Mondal, A. S. Mikhaylushkin, S. I. Simak, and I. A. Abrikosov for very useful discussions. E.Z., N.D., and L.D. acknowledge financial support of German Science Foundation (DFG) and Elite Network Bayern (ENB). R.C. acknowledges support from CINES under Grant No. stl2816.

*Author to whom correspondence should be addressed; natalia.dubrovinskaia@geow.uni-heidelberg.de

[1] P. W. Bridgman, Proc. Am. Acad. Arts Sci. **62**, 207 (1927).
[2] H. Rosner, D. Koudela, U. Schwarz, A. Handstein, M. Hanfland, I. Opahle, K. Koepernik, M. D. Kuz'min, K.-H. Müller, J. A. Mydosh, and M. Richter, Nat. Phys. **2**, 469 (2006).
[3] S. Lee, A. Pirogov, M. Kang, K.-H. Jang, M. Yonemura, T. Kamiyama, S.-W. Cheong, F. Gozzo, N. Shin, H. Kimura, Y. Noda, and J.-G. Park, Nature (London) **451**, 805 (2008).
[4] Y. W. Long, N. Hayashi, T. Saito, M. Azuma, S. Muranaka, and Y. Shimakawa, Nature (London) **458**, 60 (2009).
[5] A. Y. Kuznetsov, V. P. Dmitriev, O. I. Bandilet, and H.-P. Weber, Phys. Rev. B **68**, 064109 (2003).
[6] E. Yu. Zarechnaya, L. Dubrovinsky, N. Dubrovinskaia, N. Miyajima, Y. Filinchuk, D. Chernyshov, and V. Dmitriev, Sci. Technol. Adv. Mater. **9**, 044209 (2008).
[7] E. Yu. Zarechnaya, L. Dubrovinsky, N. Dubrovinskaia, Y. Filinchuk, D. Chernyshov, V. Dmitriev, N. Miyajima, A. El Goresy, H. F. Braun, S. Van Smaalen, I. Kantor, A. Kantor, V. Prakapenka, M. Hanfland, A. S. Mikhaylushkin, I. A. Abrikosov, and S. I. Simak, Phys. Rev. Lett. **102**, 185501 (2009).
[8] A. R. Oganov, J. Chen, C. Gatti, Y. Ma, Y. Ma, C. W. Glass, Z. Liu, T. Yu, O. O. Kurakevych, and V. L. Solozhenko, Nature (London) **457**, 863 (2009); **460**, 292 (2009).
[9] B. Albert and H. Hillebrecht, Angew. Chem., Int. Ed. **48**, 8640 (2009).
[10] T. Ogitsu, F. Gygi, J. Reed, Y. Motome, E. Schwegler, and G. Galli, J. Am. Chem. Soc. **131**, 1903 (2009).
[11] R. J. Nelmes, J. S. Loveday, D. R. Allan, J. M. Besson, G. Hamel, P. Grima, and S. Hull, Phys. Rev. B **47**, 7668 (1993).
[12] D. N. Sanz, P. Loubeyre, and M. Mezouar, Phys. Rev. Lett. **89**, 245501 (2002).
[13] M. I. Eremets, V. V. Struzhkin, H.-k. Mao, and R. J. Hemley, Science **293**, 272 (2001).
[14] X. Gonze, G.-M. Rignanese, and R. Caracas, Z. Kristallogr. **220**, 458 (2005).
[15] H. J. Monkhorst and J. D. Pack, Phys. Rev. B **13**, 5188 (1976).
[16] E. Yu. Zarechnaya, N. Dubrovinskaia, and L. Dubrovinsky, High Press. Res. **29**, 530 (2009).
[17] N. Vast, S. Baroni, G. Zerah, J. M. Besson, A. Polian, M. Grimsditch, and J. C. Chervin, Phys. Rev. Lett. **78**, 693 (1997).
[18] A. Polian, S. Ovsyannikov, M. Gauthier, P. Munsch, J.-C. Chervin, and G. Lemarchand, in *High Pressure Crystallography: From Fundamental Phenomena to Technological Applications*, edited by E. Boldyreva and P. Dera, NATO Science for Peace and Security Series B: Physics and Biophysics XIV

(Springer, Dordrecht, Netherlands, 2010), pp. 241–250.
[19] R. J. Nelmes, J. S. Loveday, R. M. Wilson, W. G. Marshall, J. M. Besson, S. Klotz, G. Hamel, T. L. Aselage, and S. Hull, Phys. Rev. Lett. **74**, 2268 (1995).
[20] E. Yu. Zarechnaya, N. Dubrovinskaia, L. Dubrovinsky, Y. Filinchuk, D. Chernyshov, and V. Dmitriev,J. Cryst. Growth **312**, 3388 (2010).
[21] Y. Le Godec, O. O. Kurakevych, P. Munsch, G. Garbarino, and V. L. Solozhenko, Solid State Commun. **149**, 1356 (2009).
[22] T. Balic-Žunić and I. Vicković, J. Appl. Crystallogr. **29**, 305 (1996).
[23] B. Johansson and S. Li, Philos. Mag. **89**, 1793 (2009).
[24] Y. Akahama, M. Kobayashi, and H. Kawamura, J. Phys. Soc. Jpn. **60**, 3211 (1991).
[25] F. Occelli, D. L. Farber, J. Badro, C. M. Aracne, D. M. Teter, M. Hanfland, B. Canny, and B. Couzinet, Phys. Rev. Lett. **93**, 095502 (2004).
[26] A. Chatterjee, A. K. Singh, and A. Jayaraman, Phys. Rev. B **6**, 2285 (1972).
[27] M. Chefki, M. M. Abd-Elmeguid, H. Micklitz, C. Huhnt, W. Schlabitz, M. Reehuis, and W. Jeitschko, Phys. Rev. Lett. **80**, 802 (1998).
[28] R. Caracas and X. Gonze, Phys. Rev. B **69**, 144114 (2004).
[29] A. Svane, P. Strange, W. M. Temmerman, Z. Szotek, H. Winter, and L. Petit, Phys. Status Solidi B **223**, 105 (2001).
[30] C. S. Yoo, B. Maddox, J.-H. P. Klepeis, V. Iota, W. Evans, A. McMahan, M. Y. Hu, P. Chow, M. Somayazulu, D. Häusermann, R. T. Scalettar, and W. E. Pickett, Phys. Rev. Lett. **94**, 115502 (2005).
[31] C. Kittel, *Einführung in die Festkörperphysik*, 9th ed. (R. Oldenbourg, München, 1991).